

# Asteroseismic Modeling of 1153 Kepler Red Giant Branch Stars

Wang, Yingxiang; Li, Tanda; Bi, Shaolan; Bedding, Timothy R.; Li, Yaguang

DOI:

[10.3847/1538-4357/ace4c9](https://doi.org/10.3847/1538-4357/ace4c9)

License:

Creative Commons: Attribution (CC BY)

*Document Version*

Publisher's PDF, also known as Version of record

*Citation for published version (Harvard):*

Wang, Y, Li, T, Bi, S, Bedding, TR & Li, Y 2023, 'Asteroseismic Modeling of 1153 Kepler Red Giant Branch Stars: Improved Stellar Parameters with Gravity-mode Period Spacings and Luminosity Constraints', *The Astrophysical Journal*, vol. 953, no. 2, 182. <https://doi.org/10.3847/1538-4357/ace4c9>

[Link to publication on Research at Birmingham portal](#)

## General rights

Unless a licence is specified above, all rights (including copyright and moral rights) in this document are retained by the authors and/or the copyright holders. The express permission of the copyright holder must be obtained for any use of this material other than for purposes permitted by law.

- Users may freely distribute the URL that is used to identify this publication.
- Users may download and/or print one copy of the publication from the University of Birmingham research portal for the purpose of private study or non-commercial research.
- User may use extracts from the document in line with the concept of 'fair dealing' under the Copyright, Designs and Patents Act 1988 (?)
- Users may not further distribute the material nor use it for the purposes of commercial gain.

Where a licence is displayed above, please note the terms and conditions of the licence govern your use of this document.

When citing, please reference the published version.






## Take down policy

While the University of Birmingham exercises care and attention in making items available there are rare occasions when an item has been uploaded in error or has been deemed to be commercially or otherwise sensitive.

If you believe that this is the case for this document, please contact [UBIRA@lists.bham.ac.uk](mailto:UBIRA@lists.bham.ac.uk) providing details and we will remove access to the work immediately and investigate.



# Asteroseismic Modeling of 1153 Kepler Red Giant Branch Stars: Improved Stellar Parameters with Gravity-mode Period Spacings and Luminosity Constraints

Yingxiang Wang (王颖翔)<sup>1,2,5</sup> , Tanda Li (李坦达)<sup>1,2,3,4,5</sup> , Shaolan Bi (毕少兰)<sup>1,2</sup> , Timothy R. Bedding<sup>4</sup> , and Yaguang Li (李亚光)<sup>4</sup> 

<sup>1</sup> Institute for Frontiers in Astronomy and Astrophysics, Beijing Normal University, Beijing 102206, People's Republic of China; [litanda@bnu.edu.cn](mailto:litanda@bnu.edu.cn)

<sup>2</sup> Department of Astronomy, Beijing Normal University, Beijing 100875, People's Republic of China

<sup>3</sup> School of Physics and Astronomy, The University of Birmingham, Birmingham B15 2TT, UK

<sup>4</sup> Sydney Institute for Astronomy (SfA), School of Physics, University of Sydney, NSW 2006, Australia

Received 2023 May 1; revised 2023 June 30; accepted 2023 June 30; published 2023 August 17

## Abstract

This paper reports the estimated stellar parameters of 1153 Kepler red giant branch stars determined with asteroseismic modeling. We use radial-mode oscillation frequencies, gravity-mode period spacings, Gaia luminosities, and spectroscopic data to characterize these stars. Compared with previous studies, we find that the two additional observed constraints, i.e., the gravity-mode period spacing and luminosity, significantly improve the precision of fundamental stellar parameters. The typical uncertainties are 2.9% for the mass, 11% for the age, 1.0% for the radius, 0.0039 dex for the surface gravity, and 0.5% for the helium core mass, making this the best-characterized large sample of red giant stars available to date. With better characterizations for these red giants, we recalibrate the seismic scaling relations and study the surface term on the red giant branch. We confirm that the surface term depends on the surface gravity and effective temperature, but there is no significant correlation with metallicity.

*Unified Astronomy Thesaurus concepts:* [Asteroseismology \(73\)](#)

*Supporting material:* machine-readable table

## 1. Introduction

NASA's Kepler mission (Borucki et al. 2008) was launched in 2008 and collected high-quality photometry data from its primary field for 4 yr. The mission allowed for the study of solar-like oscillations on nearly 20,000 red giants. Studies with the Kepler data have significantly advanced our understanding of red giants and established asteroseismology as an essential tool for precisely determining fundamental stellar parameters (see reviews by Chaplin & Miglio 2013; Hekker & Christensen-Dalsgaard 2017; Jackiewicz 2021).

The grid-based asteroseismic modeling approach has been widely used to estimate the parameters of stars (e.g., Stello et al. 2009; Kallinger et al. 2010; Basu et al. 2011). Previous research has demonstrated that accurate fundamental parameters, such as mass, radius, surface gravity, and age, can be determined by modeling the oscillation frequencies of stars (e.g., Metcalfe et al. 2010). However, it is worth noting that some estimates could be highly model-dependent, so tests for systematic bias are crucial. With this in mind, Gai et al. (2011) examined the model dependence using three different model grids, which inferred that there is almost no model dependence for inferred values of surface gravity and radius, but estimated masses and ages are model-dependent. Later on, Silva Aguirre et al. (2015) compared seven different pipelines and stated that asteroseismology could characterize main-sequence stars with

precisions of  $\sim 2\%$ ,  $\sim 4\%$ , and  $\sim 10\%$  for radius, mass, and age, respectively.

Evolved stars with different masses are crowded into a narrow red giant branch (RGB) on the H-R diagram, posing the challenge of precisely determining their fundamental parameters. Furthermore, unlike main-sequence solar-like oscillators, red giant oscillations exhibit nonradial modes of a mixed nature, making mode extraction and identification more difficult. In our previous study (Li et al. 2022, L122 hereafter), we used the radial model frequencies to determine the masses and ages of 3642 Kepler red giants. We obtained a median precision of 4.5% for mass and 16% for age. Fully using all oscillations, including mixed dipole modes, allows for even better constraints on fundamental parameters for red giants (Kallinger et al. 2008; Deheuvels et al. 2012; Li et al. 2017). Previous research demonstrated that mixed modes can constrain stellar masses and ages to precisions of  $\sim 5\%$  and  $\sim 10\%$ , respectively (Pérez Hernández et al. 2016; Zhang et al. 2018; Huber et al. 2019; Hill et al. 2021; Murphy et al. 2021). However, extracting and identifying mixed modes is time-consuming and hence difficult to apply to a large sample of stars. To effectively use the seismic information in the mixed modes and improve the modeling inferences, a compromise is to use the period spacing of the gravity dipole modes ( $\Delta\Pi$ ) extracted from the mixed modes. The value of  $\Delta\Pi$  is highly sensitive to the properties of the central core (Montalbán et al. 2013; Deheuvels et al. 2022). Given the core property is the key to understanding evolved stars,  $\Delta\Pi$  can hence provide powerful constraints for stars on the RGB (e.g., Mosser et al. 2011; Vradar et al. 2016). For instance, the distinction between hydrogen-shell burning giant stars and helium-core burning stars can be made by very different period spacings (Bedding et al. 2011). Stello et al. (2013)

<sup>5</sup> Co-first author.

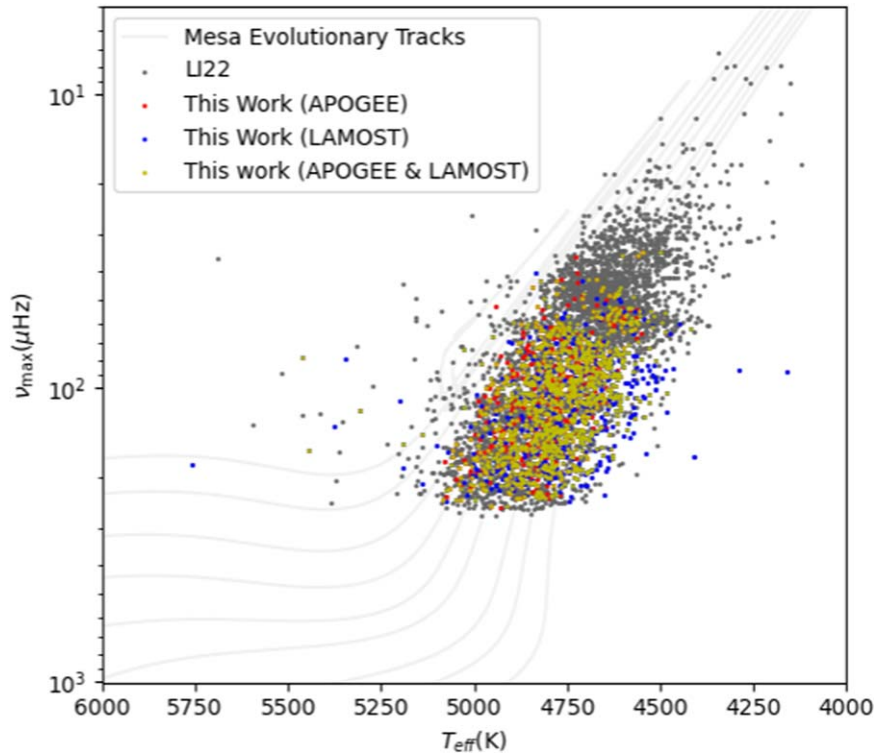


**Figure 1.** The RGB star samples in the  $T_{\text{eff}}-\nu_{\text{max}}$  diagram. Gray dots indicate the original star sample studied by LI22. The blue and red dots represent the 887 LAMOST targets and 776 APOGEE targets studied in this work, of which 510 stars are in both samples.

measured the period spacings for 13,000 Kepler targets and classified these stars into various groups such as RGB, helium-core burning clump, and secondary clump.

In this work, we aim to improve our previous seismic determinations for Kepler red giants by using the gravity-mode period spacing and Gaia luminosity as additional constraints. The rest of the paper is organized as follows: Section 2 describes our data set and modeling approach; Section 3 presents the results; we close with a summary in Section 4.

## 2. Target Selection and Modeling Approach

### 2.1. Data

In this study, the sample of Kepler RGB stars in LI22 serves as the basis for our analysis. This initial sample is composed of 3642 RGB stars with measured radial oscillation mode frequencies. It is worth noting that although they are classified as RGBs by Hon et al. (2018), we cannot be certain they are all RGBs, as asymptotic giant branch stars would have similar period spacings and be classified as RGB. We crossmatched the sample with the Kepler Red Giant Period Interval Catalog given by Vrard et al. (2016, V16, hereafter) to determine period spacings. Further, we removed stars below the so-called RGB sequence on the  $\Delta\nu-\Delta\Pi$  diagram classified by Deheuvels et al. (2022) and Rui & Fuller (2021), as these stars are assumed to have undergone mass transfer or merging events.

Utilizing the Gaia Data Release 3 catalog (Gaia Collaboration et al. 2016, 2021), we calculated luminosities,  $L$ . Given that Gaia parallaxes are known to contain zero-point offsets, we used a model from Lindegren et al. (2021) to adjust for this offset. Additionally, the reported parallaxes have underestimated uncertainties. According to external calibrations (El-Badry et al. 2021; Maíz Apellániz et al. 2021; Zinn 2021), we, therefore, increased them by a factor of 1.3. To correct for extinction, we used the

“direct” approach in the program ISOCLASSIFY (Huber et al. 2017; Berger et al. 2020), which incorporates the Green et al. (2019) dust map and the bolometric corrections from MIST models (Choi et al. 2016), to determine the luminosities by combining the parallaxes with the Two Micron All Sky Survey  $K$ -band magnitudes.

The final sample includes 1153 Kepler RGB stars, 887 of which are LAMOST targets, 776 are APOGEE targets, and 510 are common sources. In Figure 1, we show the sample on the  $T_{\text{eff}}-\nu_{\text{max}}$  diagram. Compared with the original sample, most stars below  $\nu_{\text{max}} \sim 35 \mu\text{Hz}$  are not included in this work because their  $\Delta\Pi$  values were not measured.

### 2.2. Modeling Approach

We used the stellar model grid calculated by LI22. The grid covers a mass range of  $0.76-2.20 M_{\odot}$  with four independent model input parameters: mass ( $M$ ), initial helium fraction ( $Y_{\text{init}}$ ), initial metal abundance ( $[M/H]$ ), and mixing length parameters ( $\alpha_{\text{MLT}}$ ). However, our preliminary research demonstrated that the grid’s mass resolution ( $0.02 M_{\odot}$ ) is insufficient when we have the two additional observed constraints. For this reason, we computed more models and decreased the mass step to  $0.01 M_{\odot}$ .

Before further analysis, we tested whether improving the grid resolution would significantly impact the parameter precision given by LI22. We redid the fits of LI22 using the new grid and found only slight decreases in the median uncertainties of mass (from 4.5% to 4.3%), radius (from 1.7% to 1.5%), and surface gravity (from 0.0062 to 0.0055 dex) and a slightly larger improvement in the age uncertainty (from 16% to 13%). This indicates the original grid in LI22 was slightly undersampled for estimating stellar ages.

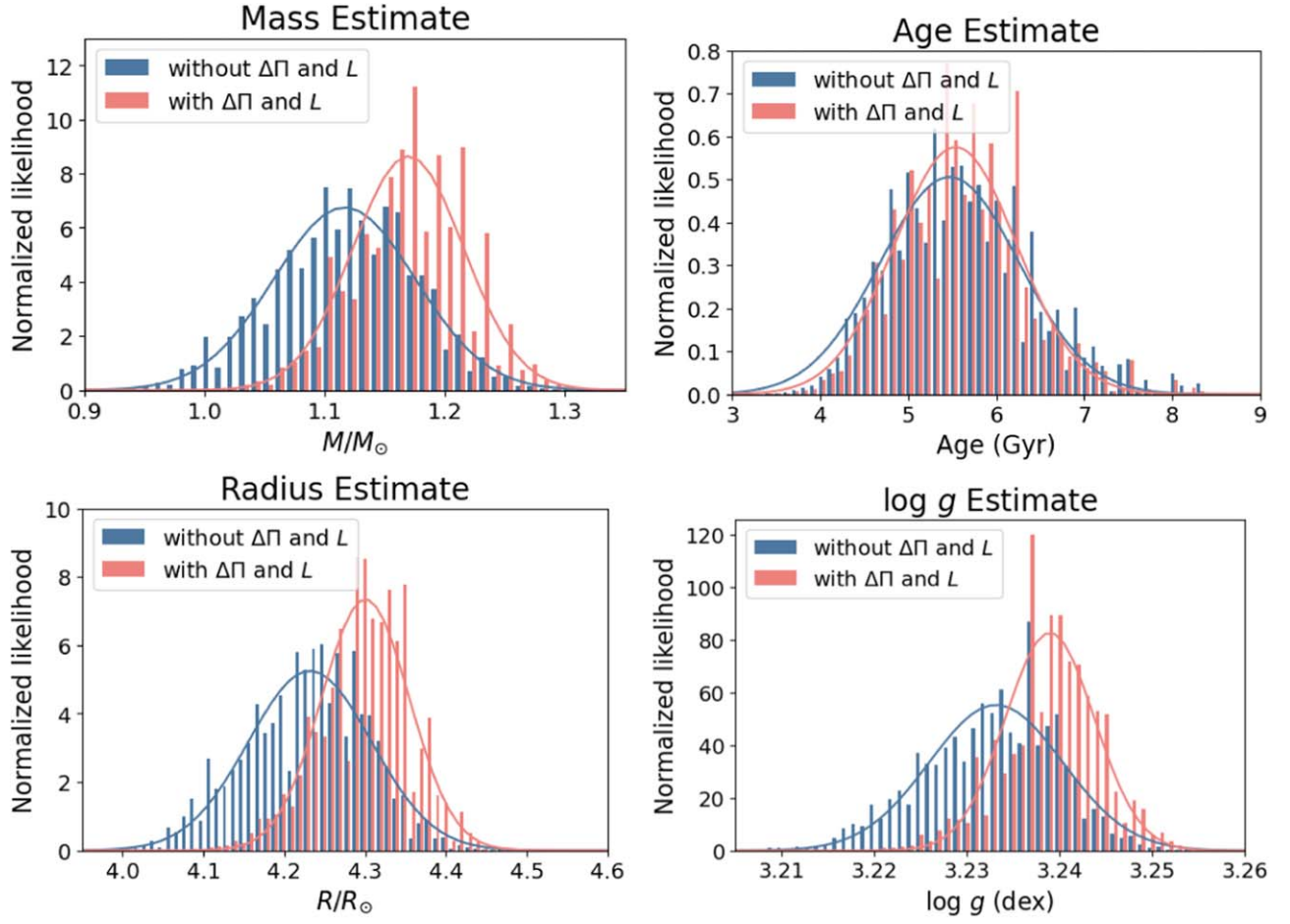


**Figure 2.** Likelihood distributions of mass, age, radius, and surface gravity for KIC 2578581. Blue bars indicate likelihood distributions determined from effective temperature, metallicity, and radial mode frequencies. Red bars represent the likelihood distributions determined with the addition of radial mode frequencies and the g-mode period spacing. The solid curves show Gaussian fits. The metallicity and effective temperature are from the APOGEE survey.

In this work, we adopted the same fitting method described by LI22. We included effective temperature ( $T_{\text{eff}}$ ), metallicity ( $[M/H]$ ), and luminosity ( $L$ ) as nonseismic observed constraints and computed the nonseismic likelihood using the following equation:

$$p_{\text{non-seismic}} = \exp \left[ -\frac{(T_{\text{eff,obs}} - T_{\text{eff,mod}})^2}{2(\sigma_{T_{\text{eff,obs}}}^2 + \sigma_{T_{\text{eff,sys}}}^2)} - \frac{([M/H]_{\text{obs}} - [M/H]_{\text{mod}})^2}{2\sigma_{[M/H]_{\text{obs}}}^2} - \frac{(L_{\text{obs}} - L_{\text{mod}})^2}{2\sigma_{L_{\text{obs}}}^2} \right], \quad (1)$$

where the subscripts “mod” and “obs” represent the model and observations, respectively. As the reported APOGEE and LAMOST uncertainties are random uncertainties, we add a systematic  $T_{\text{eff}}$  uncertainty (by adopting typical values of 2.4% reported by Tayar et al. 2022) to the random uncertainty in quadrature. Note that when the observed uncertainty of  $[M/H]$  was less than 0.1 dex, we used  $\sigma_{[M/H]_{\text{obs}}} = 0.1$  dex because of the  $[M/H]$  grid resolution. The seismic constraints were the radial mode frequencies and the asymptotic g-mode period spacing ( $\Delta\Pi$ ). The measurement of  $\Delta\Pi$  is done using the method by Vrad et al. (2016), which does not calculate  $\Delta\Pi$  after extracting all mixed-mode vibration frequencies. That is,  $\Delta\Pi$  does not represent vibration frequencies, so we treat it as

an observational measurement, and we calculated the seismic likelihood function as

$$p_{\text{seismic}} = \exp \left[ -\frac{(\Delta\Pi_{\text{obs}} - \Delta\Pi_{\text{mod}})^2}{2\sigma_{\Delta\Pi_{\text{obs}}}^2} \right] \times \prod \exp \left[ -\frac{(\nu_{i,\text{obs}} - \nu_{i,\text{mod}})^2}{2\sigma_{\nu_{i,\text{obs}}}^2} \right], \quad (2)$$

where the subscript  $i$  denotes the  $i$ th mode frequency. The final likelihood is  $p_{\text{non-seismic}} \cdot p_{\text{seismic}}$ . We estimated each stellar parameter and its uncertainty by measuring the cumulative values at 16%, 50%, and 84% on the marginal likelihood distribution. Note that we adopted the two-term formula and the method proposed by Ball & Gizon (2014) to correct the surface term in theoretical oscillation frequencies. Corrections to mode frequencies are defined as

$$\delta\nu = (a_{-1}(\nu/\nu_{\text{ac}})^{-1} + a_3(\nu/\nu_{\text{ac}})^3)/\mathcal{I}. \quad (3)$$

Here,  $\nu_{\text{ac}}$  is the acoustic cutoff frequency, which is considered to be a fixed fraction of  $\nu_{\text{max}}$  (Brown et al. 1991; Kjeldsen & Bedding 1995), and  $a_{-1}$  and  $a_3$  are free parameters. We use the fractional frequency correction at  $\nu_{\text{max}}$ , i.e.,  $\delta\nu(\nu_{\text{max}})/\nu_{\text{max}}$ , to quantify the surface term in stellar models. For each star, we

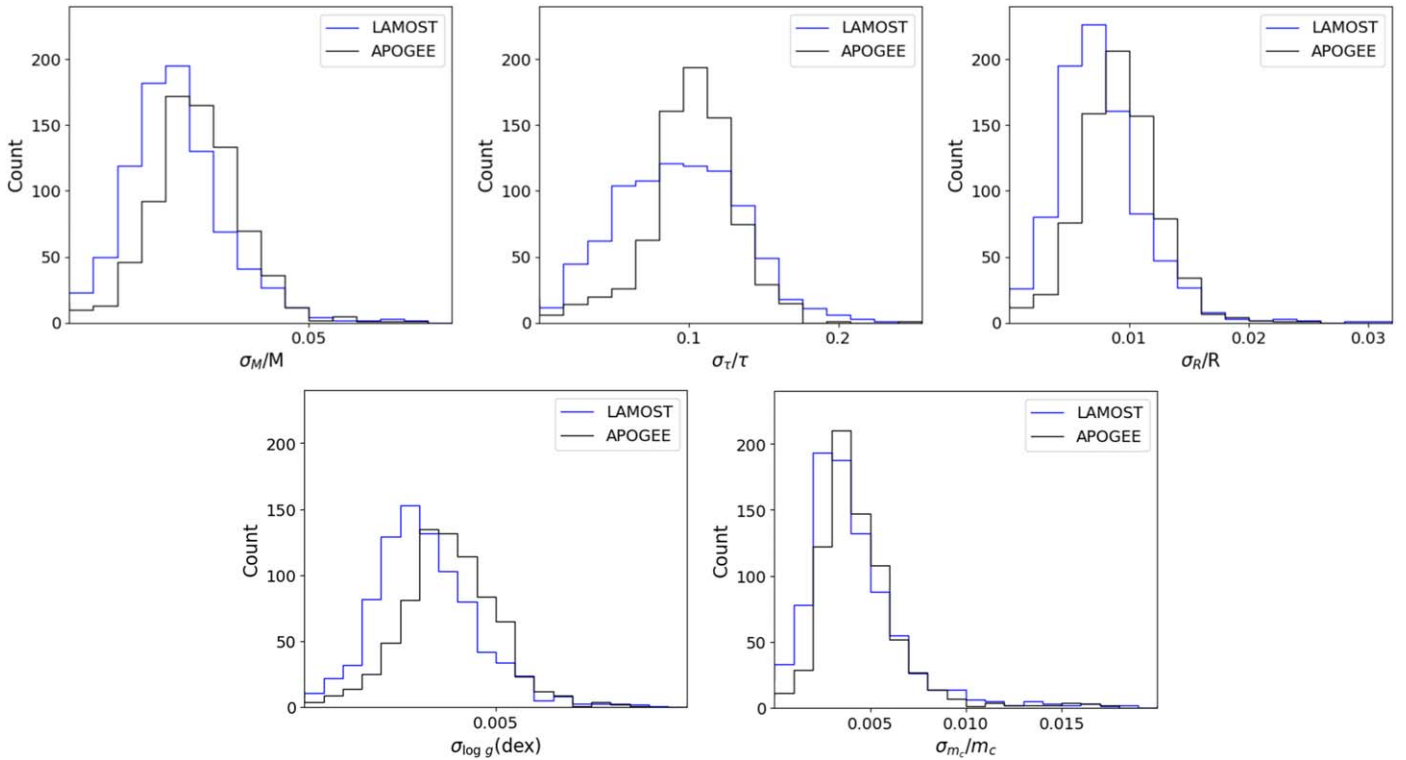


**Figure 3.** Distributions of fractional uncertainties for mass, age, radius, surface gravity, and helium core mass. Blue and black bars indicate star samples with APOGEE and LAMOST spectroscopic constraints.

**Table 1**  
Observed Constraints and Model-inferred Stellar Parameters

KIC	Source	Observed Constraints						Estimates				
		$T_{\text{eff}}$ (K)	$[M/H]$ (dex)	$\Delta\nu$ ( $\mu\text{Hz}$ )	$\nu_{\text{max}}$ ( $\mu\text{Hz}$ )	$\Delta\Pi$ (s)	$L$ ( $L_{\odot}$ )	$M$ ( $M_{\odot}$ )	$\tau$ (Gyr)	$R$ ( $R_{\odot}$ )	$\log g$ (dex)	$m_c$ ( $M_{\odot}$ )
2578581 <sup>a</sup>	APOGEE	4957	-0.181	15.95	209.2	85.9	11.5	$1.17^{+0.04}_{-0.04}$	$5.6^{+0.7}_{-0.7}$	$4.30^{+0.06}_{-0.05}$	$3.239^{+0.006}_{-0.004}$	$0.1913^{+0.0014}_{-0.0013}$
1027337	APOGEE	4636	0.231	6.94	74.2	70.1	27.3	$1.33^{+0.04}_{-0.03}$	$5.4^{+0.7}_{-0.7}$	$7.72^{+0.08}_{-0.06}$	$2.784^{+0.004}_{-0.003}$	$0.2247^{+0.0008}_{-0.0008}$
1433803	APOGEE	4736	0.236	12.18	150.1	79.3	12.1	$1.31^{+0.06}_{-0.03}$	$6.1^{+0.7}_{-1.0}$	$5.32^{+0.07}_{-0.06}$	$3.101^{+0.004}_{-0.004}$	$0.2005^{+0.0011}_{-0.0011}$
1569842	APOGEE	4820	-0.276	11.77	135.0	80.6	12.2	$1.03^{+0.02}_{-0.02}$	$9.0^{+0.6}_{-1.4}$	$5.01^{+0.04}_{-0.04}$	$3.051^{+0.003}_{-0.003}$	$0.1978^{+0.0008}_{-0.0011}$
1723752	APOGEE	5011	-0.155	15.04	197.3	83.7	12.6	$1.27^{+0.04}_{-0.04}$	$4.1^{+0.4}_{-0.5}$	$4.61^{+0.06}_{-0.05}$	$3.214^{+0.004}_{-0.004}$	$0.1963^{+0.0012}_{-0.0010}$
1723843	APOGEE	4960	-0.239	9.41	108.0	72.7	26.2	$1.43^{+0.05}_{-0.05}$	$2.4^{+0.2}_{-0.3}$	$6.52^{+0.08}_{-0.07}$	$2.964^{+0.004}_{-0.005}$	$0.2219^{+0.0013}_{-0.0009}$
1027337	LAMOST	4614	0.167	6.94	74.2	70.1	27.0	$1.35^{+0.02}_{-0.04}$	$4.8^{+0.5}_{-1.1}$	$7.78^{+0.06}_{-0.07}$	$2.787^{+0.002}_{-0.004}$	$0.2247^{+0.0009}_{-0.0007}$
1429505	LAMOST	4654	-0.152	5.76	55.8	67.9	29.2	$1.12^{+0.03}_{-0.03}$	$6.8^{+0.5}_{-0.7}$	$8.24^{+0.08}_{-0.08}$	$2.654^{+0.005}_{-0.004}$	$0.2277^{+0.0014}_{-0.0013}$
1433803	LAMOST	4690	0.176	12.18	150.1	79.3	11.8	$1.31^{+0.02}_{-0.02}$	$5.6^{+0.3}_{-0.3}$	$5.32^{+0.02}_{-0.03}$	$3.101^{+0.002}_{-0.004}$	$0.2003^{+0.0005}_{-0.0007}$
1576646	LAMOST	4778	0.001	7.67	84.5	69.6	24.8	$1.43^{+0.02}_{-0.03}$	$3.6^{+0.5}_{-0.6}$	$7.42^{+0.05}_{-0.06}$	$2.851^{+0.003}_{-0.004}$	$0.2256^{+0.0008}_{-0.0008}$
1723843	LAMOST	4902	-0.243	9.41	108.0	72.7	25.4	$1.47^{+0.03}_{-0.05}$	$2.5^{+0.2}_{-0.2}$	$6.59^{+0.05}_{-0.08}$	$2.968^{+0.003}_{-0.004}$	$0.2209^{+0.0011}_{-0.0019}$

**Note.**

<sup>a</sup> The example star in Figure 1.

(This table is available in its entirety in machine-readable form.)

used the same method to estimate  $\delta\nu(\nu_{\text{max}})/\nu_{\text{max}}$  as we used to estimate the stellar parameters.

### 3. Results

#### 3.1. Improved Stellar Parameters

We started by inspecting the improvements in likelihood distributions of stellar parameters due to the two additional constraints. Figure 2 shows comparisons between the likelihood distributions with and without  $\Delta\Pi$  and  $L$  of an example

star (KIC 2578581). The two additional constraints lead to more precise estimates of the four fundamental parameters. In LI22, the precision for the example star was 5.4% for the mass, 16% for the age, 0.015 dex for the surface gravity, and 1.8% for the radius. In this work, the precision is now improved to 3.4% for mass, 12% for age, 0.009 dex for surface gravity, and 1.2% for radius.

We estimated stellar fundamental parameters in this way for the 1153 RGB stars in our sample. Table 1 lists the observed constraints and estimated parameters. (We also



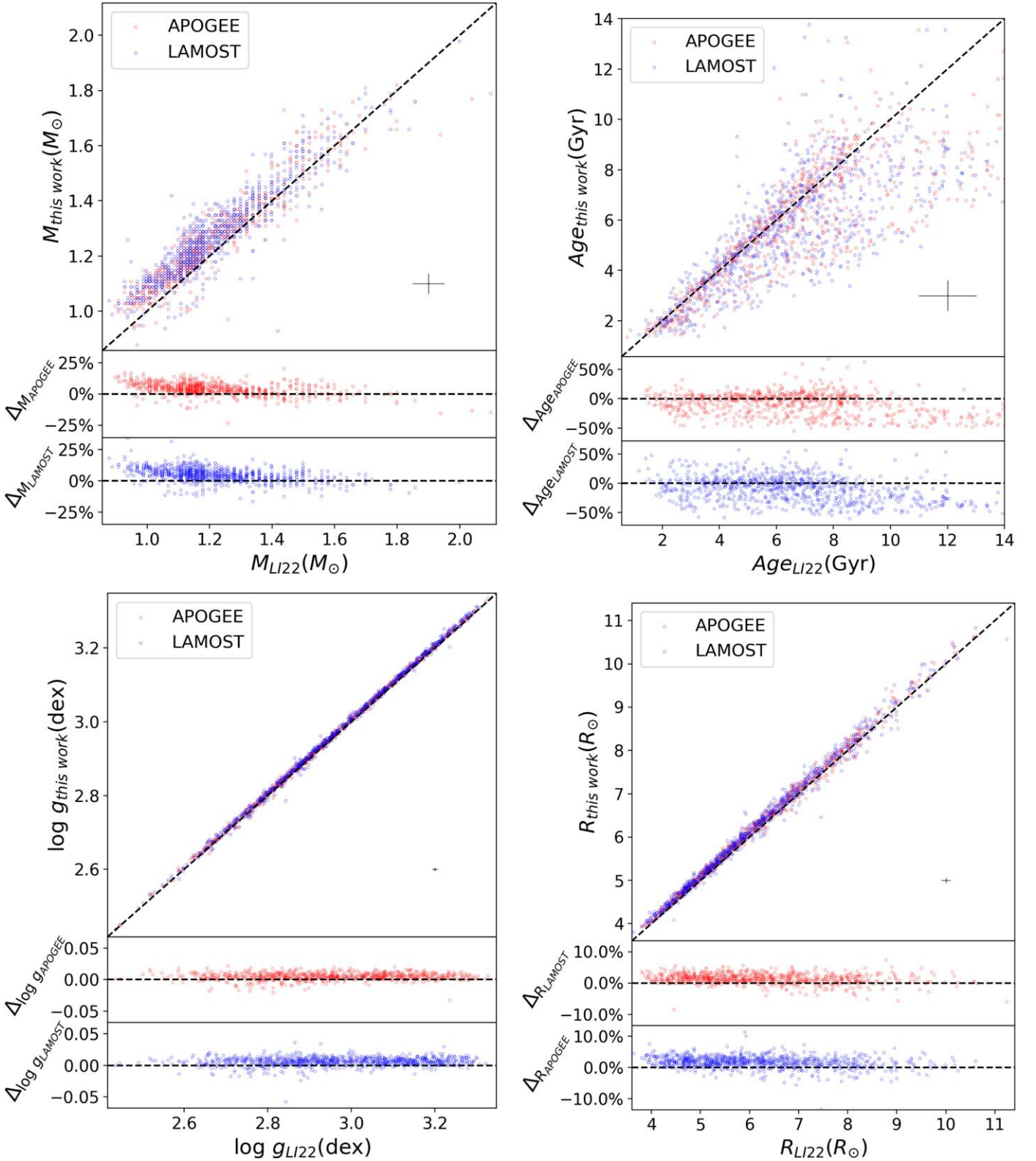


**Figure 4.** Comparison of the fitting results of the fundamental parameters from [LI22](#) and this work. For each subplot (corresponding to a fundamental parameter), the upper part is the comparison of the fitted results, and the middle and the lower parts are the differences in the fitting results for the APOGEE and LAMOST targets, respectively. The blue dots are the targets of LAMOST, and the red dots are the targets of APOGEE. In addition, each figure has a black dot with error bars, the size of which characterizes the average error of the sample.

provide the information of the example star in [Figure 1](#) at the beginning). Note there are two entries for the 510 stars that have both LAMOST and APOGEE measurements. As found

by [LI22](#), there is good agreement between the estimated parameters for stars with both LAMOST and APOGEE spectroscopic constraints. [Figure 3](#) shows the uncertainty

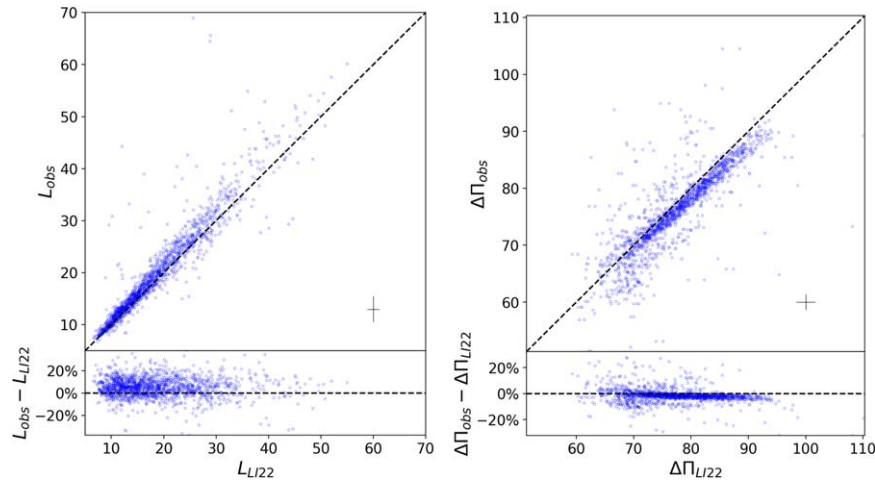


**Figure 5.** Comparison of observed and fitted values for luminosity and period spacing. The figure shows two scatterplots with error bars, one for each variable, where the  $x$ -axis is the result of fitting a stellar oscillation model (LI22) using radial mode frequency and spectral observation quantity, and the  $y$ -axis is the observed value from Gaia Data Release 3 and V16 data. This figure reveals the systematic differences between models and observations, which are also the source of the systematic differences in Figure 4.

distribution of the five stellar parameters. Interestingly, we obtained relatively high precision for the LAMOST targets because their uncertainties in  $T_{\text{eff}}$  and  $[M/H]$  are mostly smaller than those from the APOGEE survey. Given that the LAMOST spectra are lower resolution, the uncertainties may be overoptimistic compared with the APOGEE high-resolution results and the typical precision determined with the APOGEE data may be more representative for red giants. The median uncertainty of our estimates is 2.9% for mass, 11% for age, 1.0% for radius, and 0.0039 dex for  $\log g$ . In comparison to the previous results, adding the two new constraints improved the precision by a significant amount. Moreover, we estimated helium core masses, which are also listed in Table 1. The median uncertainty of helium core mass is 0.5%.

We compared our new determinations with the results in LI22 to examine systematic offsets in Figure 4. We find that our new results suggest slightly higher masses, where the average offset is 4.4%. The other offsets are  $-9.3\%$  for age, 0.005 dex for surface gravity, and 1.5% for radius. The offsets indicate that the two additional constraints bring in systematic effects. In Figure 5, we compared the modeling-inferred luminosities and  $g$ -mode period spacings given by LI22 with the observations. Apparent offsets are seen in both parameters. Observed values are slightly large for the luminosity and relatively small for the  $g$ -mode period spacing. For red giant stars, the radius and the surface gravity increase with the luminosity and are inversely proportional to the  $g$ -mode period spacing. This explains the relatively large estimates for the surface gravity and the radius. It follows that our estimated masses systematically increase due to the increased radii given the fact that the mean densities of these stars are very well constrained by radial mode frequencies.

This work has noticeably improved parameter precision compared to that of LI22. We also examined the contributions from different aspects. Table 2 lists the median precision with the old and new grids and changes for different observed constraints. We note that having luminosity as an additional constraint slightly improves the parameter precision and that the  $g$ -mode period spacing ( $\Delta\Pi$ ) has a much greater impact on the parameter precision than the luminosity ( $L$ ). Thus, the

**Table 2**  
Changes in Median Uncertainty Estimated by Different Methods

	Median Precision			
	$M$	$\tau$	$\log g$	$R$
LI22 (old grid)	4.5%	16.0%	0.0062	1.7%
new grid	4.3%	12.2%	0.0057	1.5%
new grid + $\Delta\Pi$ as an additional constraint	3.0%	11.9%	0.0040	1.0%
new grid + $L$ as an additional constraint	4.0%	11.9%	0.0053	1.4%
new grid + two additional constraints	2.9%	11.4%	0.0039	1.0%

improvements in parameter precision are mainly from the  $g$ -mode period spacing.

### 3.2. Modeling-based Scaling Relations

LI22 used modeling-inferred masses and radii to correct the scaling relations. With improved stellar parameters, we have carried out a similar analysis. The first scaling relation, in its standard form, is that  $\nu_{\text{max}}$  is proportional to  $gT_{\text{eff}}^{-0.5}$  (Brown et al. 1991; Kjeldsen & Bedding 1995). We fitted the  $\nu_{\text{max}}$  scaling relation using observed  $\nu_{\text{max}}$ ,  $T_{\text{eff}}$ ,  $[M/H]$ , and modeling-inferred  $\log g$ . For APOGEE and LAMOST targets, we derived the following results:

$$\frac{\nu_{\text{max}}}{\nu_{\text{max},\odot}} = \frac{g_{\text{fit}}}{g_{\odot}} \left( \frac{T_{\text{eff}}}{T_{\text{eff},\odot}} \right)^{-0.397} (10^{[M/H]})^{-0.008} \text{ (APOGEE)}, \quad (4)$$

and

$$\frac{\nu_{\text{max}}}{\nu_{\text{max},\odot}} = \frac{g_{\text{fit}}}{g_{\odot}} \left( \frac{T_{\text{eff}}}{T_{\text{eff},\odot}} \right)^{-0.343} (10^{[M/H]})^{-0.012} \text{ (LAMOST)}, \quad (5)$$

where the solar values are  $\nu_{\text{max},\odot} = 3090 \mu\text{Hz}$ ,  $T_{\text{eff},\odot} = 5777 \text{ K}$ , and  $\log g_{\odot} = 4.44$  (Huber et al. 2011). Compared to the scaling relations in LI22, we found the same power law for the  $g$  term, but the exponents for the  $T_{\text{eff}}$  and  $[M/H]$  terms are marginally different (LI22 gave  $-0.459$  and  $-0.022$  for APOGEE, and  $-0.421$  and  $-0.039$  for LAMOST). Our updated version

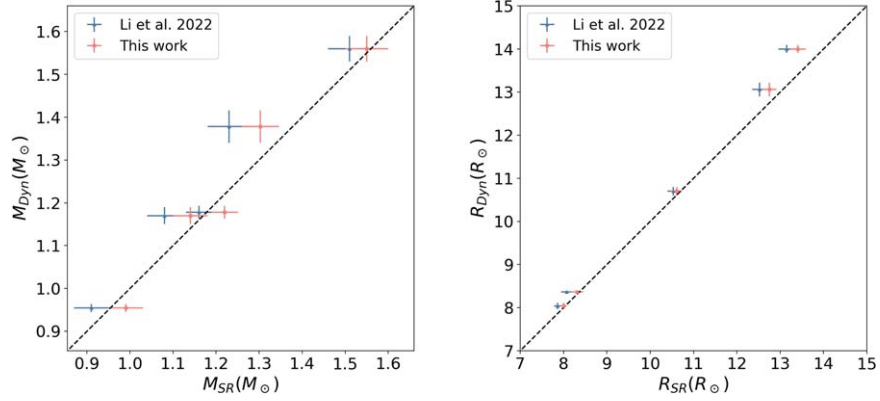


**Figure 6.** Comparison between the masses and radii of five red giants in binary systems derived from dynamical models and corrected scaling relations. The left panel shows the difference between the two methods for the masses of each star. The right panel shows the same for the radii. The blue points use the corrected scaling relations from LI22, while the red points use the corrected scaling relations from this work.

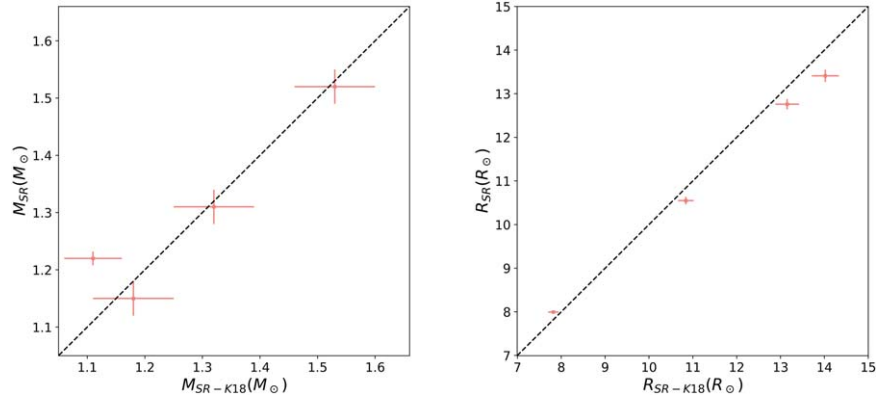


**Figure 7.** Comparison between the masses and radii of four red giants in binary systems derived from dynamical models and corrected scaling relations. The left panel shows the difference between the two methods for the masses of each star. The right panel shows the same for the radii. The horizontal coordinate uses the corrected scaling relations from Kallinger et al. (2018), while the ordinate uses the corrected scaling relations from this work.

suggests values closer to the standard scaling relation, with very little dependence on metallicity.

The second standard scaling relation is that the large frequency separation of radial modes,  $\Delta\nu$ , is proportional to the square root of the mean stellar density (Ulrich 1986). We used the observed  $\Delta\nu$  and the model-determined mean density to fit the  $\Delta\nu$  scaling relation and obtained

$$\frac{\Delta\nu}{\Delta\nu_{\odot}} = \left( \frac{\bar{\rho}_{\text{fit}}}{\bar{\rho}_{\odot}} \right)^{0.507}, \quad (6)$$

where  $\Delta\nu_{\odot} = 135.1 \mu\text{Hz}$ . This result is identical to that given by LI22, indicating that the  $\Delta\nu$  scaling relation is not sensitive to the systematic offset in estimated masses.

To test the accuracy of the scaling relations after applying corrections for various effects, we used a sample of five red giants in eclipsing binary systems, whose masses and radii are accurately measured by dynamical modeling. The five red giants are KIC 8410637 (Frandsen et al. 2013), KIC 9970396, KIC 7037405, KIC 9540226 (Brogaard et al. 2018), and KIC 4054905 (Brogaard et al. 2022). They all have high-resolution spectra from APOGEE, allowing us to use the corrected scaling relations calibrated for APOGEE data. We compared our results with those from the corrected scaling relations of LI22. Figure 6 shows that our new scaling relations yield masses within  $1\sigma$  of the dynamical masses for three red

giants and within  $1.5\sigma$  for the other two, and significantly improve the accuracy of mass and radius estimation compared to LI22’s scaling relations. Kallinger et al. (2018) used four of the mentioned eclipsing binary red giants, KIC 8410637, KIC 9970396, KIC 7037405, and KIC 9540226. They used these stars to revise the scaling relations, so we use their results as a reference for our corrected scaling relations. Figure 7 shows that our new scaling relations yield masses within  $1.5\sigma$  of the seismic masses, using the corrected scaling relations from Kallinger et al. (2018) for these red giants.

### 3.3. Surface Term

The surface term in asteroseismology refers to the differences between observed oscillation frequencies and those of the best-fitting model (Christensen-Dalsgaard 1982). The surface term is caused by incorrect modeling of the near-surface layers in stellar code. Given that the properties’ near-surface layers largely correlate to global parameters, the surface term is expected to vary smoothly as a function of effective temperature, surface gravity, and metallicity (Trampedach et al. 2017; Compton et al. 2018; Jørgensen et al. 2020; Ong et al. 2021; Li et al. 2023). The star sample in this work makes it possible to systematically study the surface term and its dependencies on surface features in a wide parameter range.



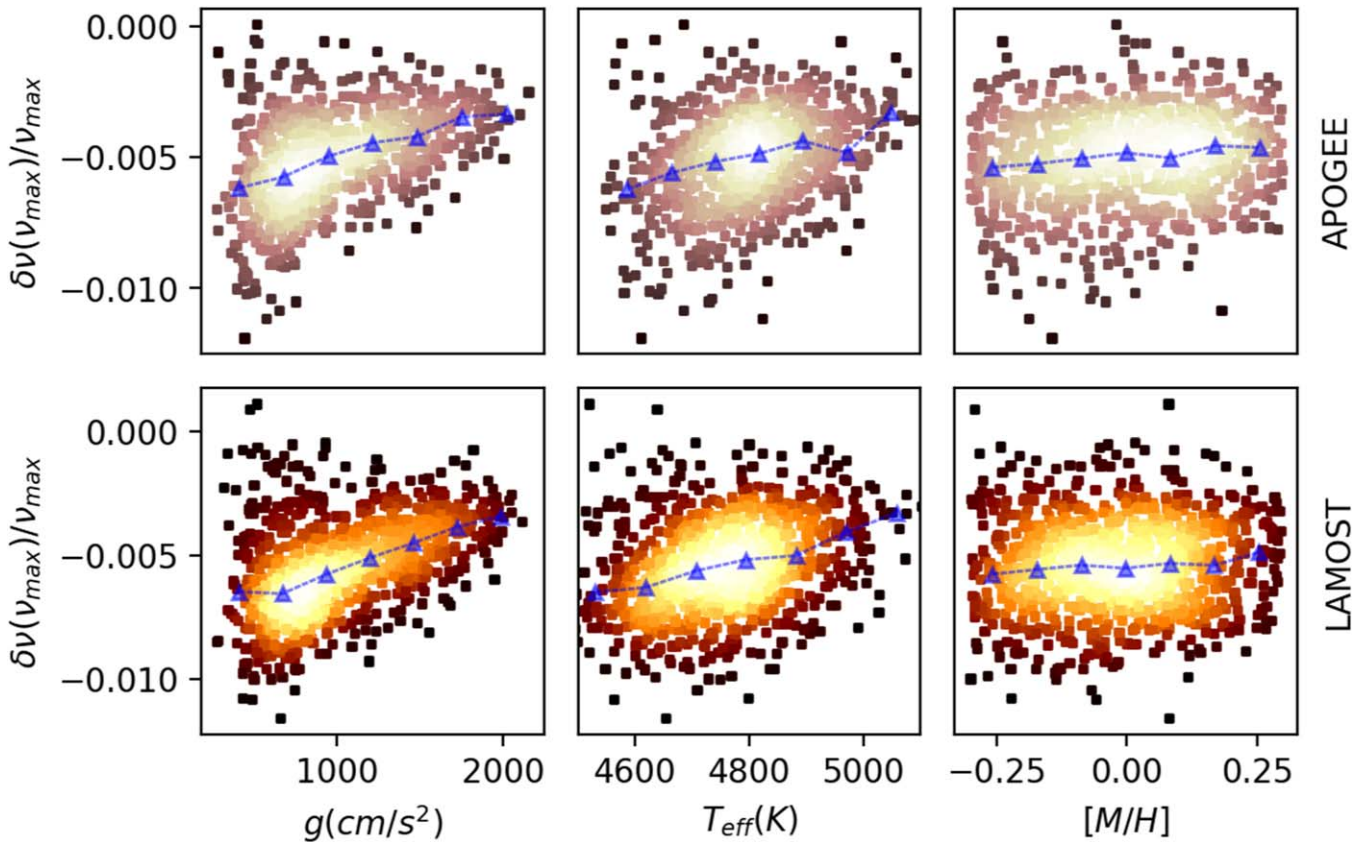


**Figure 8.** Density scatterplots of the surface correction with three stellar parameters. The top row of subplots shows stars observed by the APOGEE, and the bottom row shows the LAMOST targets. The filled triangle represents the middle value of each bin.

We investigated the correlations between  $\delta\nu(\nu_{\max})/\nu_{\max}$  and three parameters, i.e., seismic surface gravity ( $g$ ), effective temperature ( $T_{\text{eff}}$ ), and metallicity ( $[M/H]$ ), in Figure 8. We found that the surface term strongly depends on the surface gravity and effective temperature, but there is no significant correlation with metallicity. We fitted  $\delta\nu(\nu_{\max})/\nu_{\max}$  as a function of two surface parameters using the formula as follows:

$$\frac{\delta\nu(\nu_{\max})}{\nu_{\max}} = \beta_0 \left( \frac{g}{g_{\odot}} \right)^{\beta_1} \left( \frac{T_{\text{eff}}}{T_{\text{eff},\odot}} \right)^{\beta_2}. \quad (7)$$

We used the `scipy curve_fit` module and found the best-fitting parameters are  $[\beta_0, \beta_1, \beta_2] = [-0.0014 \pm 0.0002, -0.32 \pm 0.04, -1.1 \pm 0.7]$  with the APOGEE  $T_{\text{eff}}$  and  $[M/H]$ , and  $[\beta_0, \beta_1, \beta_2] = [-0.0016 \pm 0.0002, -0.26 \pm 0.03, -1.7 \pm 0.4]$  with the LAMOST data. We also calculated the residual between fitting and true value. After analyzing the residual, we still failed to find any correlation with metallicity. Moreover, the absolute value of  $\delta\nu(\nu_{\max})/\nu_{\max}$  is relatively large for stars with lower surface gravity, indicating that the surface effect increases with stars' evolution on the RGB.

#### 4. Conclusions

As a follow-up study of LI22, we have introduced two additional observed constraints to improve the estimated fundamental parameters of a sample of Kepler red giants. We notice that the gravity-mode period spacing and Gaia luminosity significantly improve the precision of 1153 red

giant branch stars. The typical uncertainty is 2.9% for the mass, 11% for the age, 1.0% for the radius, 0.0039 dex for the surface gravity, and 0.5% for the helium core mass, making this the best-characterized sample of red giant stars available to date.

With the improved stellar parameters, we rederive the seismic scaling relations. Compared with our previous version, the updated  $\nu_{\max}$  scaling relation suggests a relatively small dependence on the effective temperature and the metallicity. Moreover, we systematically study the surface term for red giant stars. The results indicate that the surface term increases when stars become more evolved on RGB. The surface term strongly depends on the surface gravity and effective temperature, but we find no significant correlation with metallicity.

#### Acknowledgments

This work is supported by the National Natural Science Foundation of China (NSFC) (grants 12090040, 12090042) and the Joint Research Fund in Astronomy (U2031203) under cooperative agreement between the National Natural Science Foundation of China (NSFC) and Chinese Academy of Sciences (CAS). This work is also supported by the Fundamental Research Funds for the Central Universities. This paper has also received funding from the European Research Council (ERC) under the European Unions Horizon 2020 research and innovation program (Cartography GA. 804752). T.R.B. acknowledges support from the Australian Research Council through Laureate Fellowship FL220100117. We also thank the Kepler team for making this research possible.

## ORCID iDs

Yingxiang Wang (王颖翔)  <https://orcid.org/0000-0003-4721-1668>  
 Tanda Li (李坦达)  <https://orcid.org/0000-0001-6396-2563>  
 Shaolan Bi (毕少兰)  <https://orcid.org/0000-0002-7642-7583>  
 Timothy R. Bedding  <https://orcid.org/0000-0001-5222-4661>  
 Yaguang Li (李亚光)  <https://orcid.org/0000-0003-3020-4437>

## References

- Ball, W. H., & Gizon, L. 2014, *A&A*, **568**, A123  
 Basu, S., Grundahl, F., Stello, D., et al. 2011, *ApJL*, **729**, L10  
 Bedding, T. R., Mosser, B., Huber, D., et al. 2011, *Natur*, **471**, 608  
 Berger, T. A., Huber, D., van Saders, J. L., et al. 2020, *AJ*, **159**, 280  
 Borucki, W., Koch, D., Batalha, N., et al. 2008, in IAU Symp. 4, *Transiting Planets* (Cambridge: Cambridge Univ. Press), 289  
 Brogaard, K., Arentoft, T., Slumstrup, D., et al. 2022, *A&A*, **668**, A82  
 Brogaard, K., Hansen, C., Miglio, A., et al. 2018, *MNRAS*, **476**, 3729  
 Brown, T. M., Gilliland, R. L., Noyes, R. W., & Ramsey, L. W. 1991, *ApJ*, **368**, 599  
 Chaplin, W. J., & Miglio, A. 2013, *ARA&A*, **51**, 353  
 Choi, J., Dotter, A., Conroy, C., et al. 2016, *ApJ*, **823**, 102  
 Christensen-Dalsgaard, J. 1982, *MNRAS*, **199**, 735  
 Compton, D. L., Bedding, T. R., Ball, W. H., et al. 2018, *MNRAS*, **479**, 4416  
 Deheuvels, S., Ballot, J., Gehan, C., & Mosser, B. 2022, *A&A*, **659**, A106  
 Deheuvels, S., García, R. A., Chaplin, W. J., et al. 2012, *ApJ*, **756**, 19  
 El-Badry, K., Rix, H.-W., & Heintz, T. M. 2021, *MNRAS*, **506**, 2269  
 Frandsen, S., Lehmann, H., Hekker, S., et al. 2013, *A&A*, **556**, A138  
 Gai, N., Basu, S., Chaplin, W. J., & Elsworth, Y. 2011, *ApJ*, **730**, 63  
 Green, G. M., Schlafly, E., Zucker, C., Speagle, J. S., & Finkbeiner, D. 2019, *ApJ*, **887**, 93  
 Gaia Collaboration, Brown, A. G. A., & Vallenari, A. 2021, *A&A*, **649**, A1  
 Gaia Collaboration, Prusti, T., & de Bruijne, J. H. J. 2016, *A&A*, **595**, A1  
 Hekker, S., & Christensen-Dalsgaard, J. 2017, *A&ARv*, **25**, 1  
 Hill, M. L., Kane, S. R., Campante, T. L., et al. 2021, *AJ*, **162**, 211  
 Hon, M., Stello, D., & Yu, J. 2018, *MNRAS*, **476**, 3233  
 Huber, D., Bedding, T. R., Stello, D., et al. 2011, *ApJ*, **743**, 143  
 Huber, D., Chaplin, W. J., Chontos, A., et al. 2019, *AJ*, **157**, 245  
 Huber, D., Zinn, J., Bojsen-Hansen, M., et al. 2017, *ApJ*, **844**, 102  
 Jackiewicz, J. 2021, *FrASS*, **7**, 595017  
 Jørgensen, A. C. S., Montalbán, J., Miglio, A., et al. 2020, *MNRAS*, **495**, 4965  
 Kallinger, T., Beck, P. G., Stello, D., & García, R. A. 2018, *A&A*, **616**, A104  
 Kallinger, T., Guenther, D. B., Matthews, J. M., et al. 2008, *A&A*, **478**, 497  
 Kallinger, T., Mosser, B., Hekker, S., et al. 2010, *A&A*, **522**, A1  
 Kjeldsen, H., & Bedding, T. R. 1995, *A&A*, **293**, 87  
 Li, T., Bedding, T. R., Huber, D., et al. 2017, *MNRAS*, **475**, 981  
 Li, T., Li, Y., Bi, S., et al. 2022, *ApJ*, **927**, 167  
 Li, Y., Bedding, T. R., Stello, D., et al. 2023, *MNRAS*, **523**, 916  
 Lindegren, L., Bastian, U., Biermann, M., et al. 2021, *A&A*, **649**, A4  
 Maíz Apellániz, J., Pantaleoni González, M., & Barbá, R. H. 2021, *A&A*, **649**, A13  
 Metcalfe, T. S., Monteiro, M., Thompson, M. J., et al. 2010, *ApJ*, **723**, 1583  
 Montalbán, J., Miglio, A., Noels, A., et al. 2013, *ApJ*, **766**, 118  
 Mosser, B., Barban, C., Montalbán, J., et al. 2011, *A&A*, **532**, A86  
 Murphy, S. J., Li, T., Sekaran, S., et al. 2021, *MNRAS*, **505**, 2336  
 Ong, J. M. J., Basu, S., & McKeever, J. M. 2021, *ApJ*, **906**, 54  
 Pérez Hernández, F., García, R. A., Corsaro, E., Triana, S. A., & De Ridder, J. 2016, *A&A*, **591**, A99  
 Rui, N. Z., & Fuller, J. 2021, *MNRAS*, **508**, 1618  
 Silva Aguirre, V., Davies, G., Basu, S., et al. 2015, *MNRAS*, **452**, 2127  
 Stello, D., Chaplin, W. J., Bruntt, H., et al. 2009, *ApJ*, **700**, 1589  
 Stello, D., Huber, D., Bedding, T. R., et al. 2013, *ApJL*, **765**, L41  
 Tayar, J., Clayton, Z. R., Huber, D., & van Saders, J. 2022, *ApJ*, **927**, 31  
 Trampedach, R., Aarslev, M. J., Houdek, G., et al. 2017, *MNRAS*, **466**, L43  
 Ulrich, R. K. 1986, *ApJL*, **306**, L37  
 Vrad, M., Mosser, B., & Samadi, R. 2016, *A&A*, **588**, A87  
 Zhang, X., Wu, T., & Li, Y. 2018, *ApJ*, **855**, 16  
 Zinn, J. C. 2021, *AJ*, **161**, 214